Digital Signal Processing 34 (2014) 67–73

Contents lists available at ScienceDirect

Digital Signal Processing

www.elsevier.com/locate/dsp

High-precision frequency estimation of real sinusoids with reduced computational complexity using a model-based matched-spectrum approach

Alessandro J.S. Dutra [a], José F.L. de Oliveira [a], Thiago de M. Prego [a,b,*], Sergio L. Netto [a], Eduardo A.B. da Silva [a]

[a] Program of Electrical Engineering, COPPE, Federal University of Rio de Janeiro, RJ, Brazil
[b] Postgraduate Program of Electrical Engineering, Federal Center for Technological Education Celso Suckow da Fonseca (CEFET-RJ), Nova Iguaçu, RJ, Brazil

ARTICLE INFO

Article history:
Available online 1 August 2014

Keywords:
Frequency estimation
Real sinusoid
Model-based approach
Matched spectrum

ABSTRACT

Frequency-estimation algorithms devised for complex sinusoids, including the maximum-likelihood (ML) approach, when operating on real sinusoidal signals, suffer from spectral interference due to the superposition of the aliasing components at negative and positive frequencies. This paper introduces a frequency estimation ML-like algorithm, based on a spectral-matching approach, that avoids such superposition effect by incorporating it in the signal/spectrum model. As a result, the proposed method is able to generate a more precise frequency estimate in comparison to previous approaches at a comparable computational cost, as endorsed by provided computational analyses and simulation results.

1. Introduction

Frequency estimation is a standard problem in the signal processing field with a plethora of applications ranging from radar and satellite/mobile communications to general audio or speech processing and metrology [1–5]. The theoretical basis for the optimal frequency estimation, based on the maximum-likelihood (ML) criterion, of a discrete-time complex sinusoid embedded in noise was established in [6]. Later on, a series of algorithms based on the interpolation of the signal spectrum was devised to reduce the associated computational cost [7–15]. Generally speaking, all interpolation methods are computationally simple, requiring just a few operations in addition to the initial discrete Fourier transform (DFT) computation, and provide a very good ML approximation. They all, however, were initially devised for noisy complex-sinusoid signals, and, therefore, when dealing with real sinusoids, suffer from spectral superposition of the positive and negative frequency complex sinusoids, which introduces estimation bias and increases estimation variance.

To overcome such issues, a new frequency-estimation algorithm is considered based on a matched-spectrum concept, which correlates the measured DFT with the theoretical spectrum of a sampled sinusoid. The result is a new estimation method which yields very precise frequency estimates, particularly for high signal-to-noise ratios (SNR), at a reduced (comparable to the spectrum-interpolation algorithms) computational cost, as verified by computer simulations. In addition, both its estimation accuracy and robustness to noise can be scaled at the expense of increased computational complexity.

To introduce the proposed matched-spectrum (MS) method, this paper is organized as follows. Sections 2 and 3 revisit the ML and interpolation methods for frequency estimation, respectively. The proposed MS algorithm is introduced in Section 4, whereas Section 5 discusses some practical considerations on its implementation and performance. Section 6 includes some computational experiments illustrating the interesting results achieved by the proposed algorithm in comparison to previous schemes. Finally, Section 7 concludes the paper summarizing its technical contributions.

2. Maximum-likelihood estimation

Assume a complex sinusoid $s(n) = \tilde{a}\exp j(\tilde{\omega}n + \tilde{\theta})$, of amplitude $\tilde{a}$, frequency $\tilde{\omega}$, and phase $\tilde{\theta}$, is immersed in additive white Gaussian noise $v(n) = v_R(n) + jv_I(n)$, whose imaginary part $v_I(n)$ is the Hilbert transform of its real part $v_R(n)$. Assume also that

* Correspondence to: CEFET-RJ UnED Nova Iguaçu, Estrada de Adrianópolis, 1.317, Santa Rita, Nova Iguaçu – RJ – 26041-271.
E-mail addresses: alessandro.dutra@smt.ufrj.br (A.J.S. Dutra), jose.oliveira@smt.ufrj.br (J.F.L. de Oliveira), thiago.prego@smt.ufrj.br (T. de M. Prego), sergioln@smt.ufrj.br (S.L. Netto), eduardo@smt.ufrj.br (E.A.B. da Silva).

http://dx.doi.org/10.1016/j.dsp.2014.07.017
1051-2004/

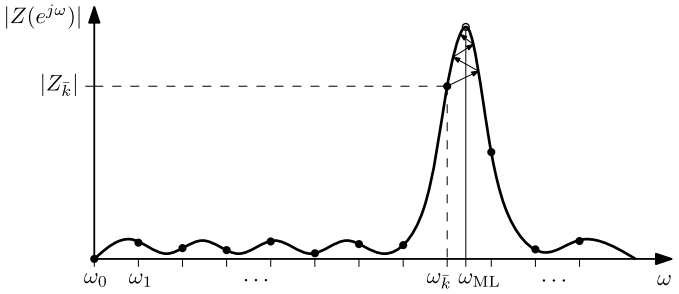

Fig. 1. ML frequency estimation ω_{ML} using the absolute value of the DFT: starting at the peak position $\omega_{\bar{k}}$ of $|Z(e^{j\omega_k})|$, estimate refinement is performed by numerical optimization of periodogram function, as given in Eq. (3).

$v(n)$ has zero mean and variance σ_v^2. The corresponding sample vector $\mathbf{z} = [z(0)z(1)\ldots z(N-1)]^{\mathrm{T}}$, where $z(n) = s(n) + v(n)$, has the joint distribution

$$f_{\mathbf{z}}(\mathbf{p}) = \left(\frac{1}{\sqrt{2\pi\sigma_v^2}}\right)^N e^{-\frac{1}{2\sigma_v^2}\sum_{n=0}^{N-1}[(x(n)-\mu_{\mathbf{p}}(n))^2+(y(n)-\nu_{\mathbf{p}}(n))^2]}, \quad (1)$$

where $\mathbf{p} = [a, \omega, \theta]^{\mathrm{T}}$ is the parameter vector, $x(n)$ and $y(n)$ are the real and imaginary parts of $z(n)$, respectively, and

$$\mu_{\mathbf{p}}(n) = \tilde{a}\cos(\tilde{\omega}n + \tilde{\theta}), \qquad \nu_{\mathbf{p}}(n) = \tilde{a}\sin(\tilde{\omega}n + \tilde{\theta}). \quad (2)$$

The maximum-likelihood (ML) parameter estimator $\mathbf{p}_{\mathrm{ML}} = [a_{\mathrm{ML}}, \omega_{\mathrm{ML}}, \theta_{\mathrm{ML}}]^{\mathrm{T}}$ of $\mathbf{p}$, given the observations $\mathbf{z}$, is the value of $\mathbf{p}$ that maximizes $f_{\mathbf{z}}(\mathbf{p})$ given in Eq. (1). After some algebraic development, one has that [6]:

- ω_{ML} is the value of ω that maximizes the periodogram

$$|A(\omega)| = \left|\frac{1}{N}\sum_{n=0}^{N-1} z(n)e^{-j\omega n}\right|. \quad (3)$$

- θ_{ML} is the argument of $A(\omega_{\mathrm{ML}})$.
- $a_{\mathrm{ML}} = |A(\omega_{\mathrm{ML}})|$.

These results suggest a simple strategy for estimating the ML parameters:

1. Determine the discrete Fourier transform (DFT), $Z(e^{j\omega_k})$, of the sequence $\mathbf{z}$ and determine the (discrete) frequency value $\omega_{\bar{k}}$ associated with the maximum of its absolute value [16].
2. Starting at $\omega_{\bar{k}}$, use some numerical optimization algorithm to maximize $|A(\omega)|$ in Eq. (3) to determine ω_{ML} [6], as illustrated in Fig. 1.
3. Once ω_{ML} is estimated, compute $\theta_{\mathrm{ML}} = \arg\{A(\omega_{\mathrm{ML}})\}$ and $a_{\mathrm{ML}} = |A(\omega_{\mathrm{ML}})|$, as indicated above.

3. Fine adjustment by interpolation

Obtaining the ML estimate by optimizing the periodogram, besides being a cumbersome procedure due to the nature of the function evaluated at each iteration, may also not always converge to the desired solution, as analyzed in [17]. An alternative approach, which is quite simple and robust, is based on the interpolation of the DFT mainlobe points, which enables us to estimate the frequency deviation δ such that $\omega_{\mathrm{ML}} = \omega_{\bar{k}} + \delta$, as indicated in Fig. 2.

Among the several interpolation-based approaches found in the literature [7–15], one of the most successful employs [13]

$$\frac{\hat{\delta}}{\Delta} = \frac{\sqrt{1+8\gamma^2}-1}{4\gamma}, \quad (4)$$

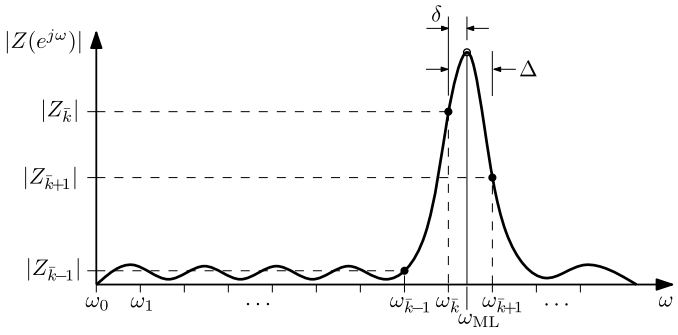

Fig. 2. ML frequency estimation ω_{ML} using the absolute value of the DFT: starting at the peak position $\omega_{\bar{k}}$ of $|Z(e^{j\omega_k})|$, a frequency deviation δ is estimated by interpolation of side points at $\omega_{\bar{k}-1}$ and $\omega_{\bar{k}+1}$.

where $\Delta = \frac{2\pi F_s}{N}$ is the DFT frequency resolution (with the sampling frequency F_s in samples per second), as represented in Fig. 2, and

$$\gamma = \frac{R_{-1} - R_1}{2R_0 + R_{-1} + R_1}, \quad (5)$$

with R_k, for $k \in \mathbb{Z}$, being defined as

$$R_k = \mathrm{real}\{Z(e^{j\omega_{\bar{k}+k}}) \times \mathrm{conj}\{Z(e^{j\omega_{\bar{k}}})\}\}, \quad (6)$$

where $\mathrm{conj}\{\cdot\}$ denotes the complex-conjugate operation. An extension of this interpolator which employs four neighboring points and the periodogram peak at $\omega_{\bar{k}}$ is also presented in [13], with slightly superior computational complexity and estimation performance.

All these complex-sinusoid based algorithms, including the recent proposal given in [14], suffer from spectral leakage due to the spectral component centered at $\omega = -\tilde{\omega}$. This generates some bias on the final frequency estimate of real-sinusoid signals. The proposed method attempts to prevent this issue using a model-based approach, as described in the following section.

4. Proposed method: matched spectrum

The proposed matched-spectrum (MS) scheme attempts to match the DFT of the observation data, as determined in the first stage of all previous algorithms, to the theoretical spectrum $S_{\tilde{\omega},\tilde{\theta}}(e^{j\omega_k})$ of a frequency-$\tilde{\omega}$ and phase-$\tilde{\theta}$ sinusoid sampled at the same DFT frequency values ω_k. For that matter, one searches for the optimal values $\tilde{\omega}$ of ω and $\tilde{\theta}$ of θ that maximize the correlation

$$\tilde{R}_{k_0}(\omega,\theta) = \frac{\sum_{k=-k_0}^{k_0} Z(e^{j\omega_{\bar{k}+k}}) \times \mathrm{conj}\{S_{\omega,\theta}(e^{j\omega_{\bar{k}+k}})\}}{\sqrt{\sum_{k=-k_0}^{k_0} S_{\omega,\theta}(e^{j\omega_{\bar{k}+k}}) \times \mathrm{conj}\{S_{\omega,\theta}(e^{j\omega_{\bar{k}+k}})\}}}, \quad (7)$$

where k_0 is the interval of interest around $\bar{k}$. In practice, this correlation function has the following interesting properties:

- In the noiseless case, it has a global maximum at $\omega = \tilde{\omega}$ and $\theta = \tilde{\theta}$.
- When $\omega \approx \tilde{\omega}$ and $\theta \approx \tilde{\theta}$, it does not present local minima, even in the presence of noise, as illustrated in Section 6, allowing a simple line-search procedure to determine $\tilde{\omega}$ and $\tilde{\theta}$ with a very high precision.
- Its value is readily approximated even for small values of k_0, including the trivial case $k_0 = 1$.
- For given values of ω and θ, its evaluation requires only $2(2k_0 + 1)$ complex multiplications and a single complex division (see detailed algorithm at the end of this section), in contrast to the periodogram function defined in Eq. (3), whose complexity is linear with the number of signal samples N.

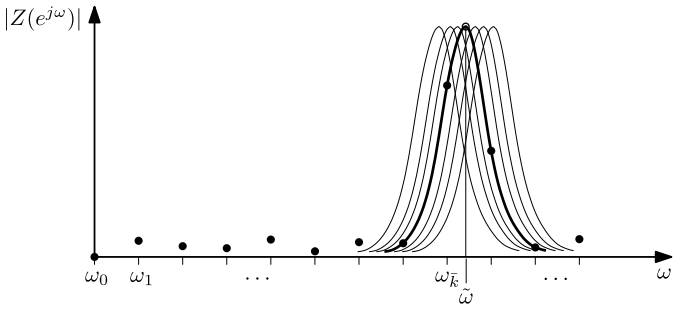

Fig. 3. Proposed frequency estimation with iterative refinement by matching theoretical spectrum (continuous lines) to practical data (scattered dots).

- Its maximization with respect to ω and θ works like a frequency-domain counterpart of the ML matched filter detector used in communications systems, as illustrated in Fig. 3.

The complex-sinusoid $s(n) = \tilde{a}\exp j(\tilde{\omega}n + \tilde{\theta})$ considered up to this point is very important in the theoretical sense, as it enables a simpler analysis of the estimation problem, as provided above. Most practical applications, however, involve a real-sinusoid signal $s(n) = \tilde{a}\cos(\tilde{\omega}n + \tilde{\theta})$ in the presence of noise. In such cases, the signal theoretical spectrum, as required in Eq. (7), may be determined in a closed form to avoid extra DFT calculations such that [18]:

$$S_{\tilde{\omega},\tilde{\theta}}\left(e^{j\omega_k}\right) = \frac{\tilde{a}}{2}\left[e^{j\tilde{\theta}}g(\omega_k - \tilde{\omega}) + e^{-j\tilde{\theta}}g(\omega_k + \tilde{\omega})\right], \tag{8}$$

with $g(\Omega)$ being the Fourier transform of the window used for the DFT calculation. When a rectangular window is used,

$$g(\Omega) = e^{-\frac{j\Omega(N-1)}{2}}\left(\frac{\sin\frac{\Omega N}{2}}{\sin\frac{\Omega}{2}}\right). \tag{9}$$

A major difficulty of employing Eqs. (8) and (9) is that an estimate $\hat{\omega}$ of the true frequency $\tilde{\omega}$ depends on the true phase component $\tilde{\theta}$, whose estimate $\hat{\theta}$, on its own turn, is highly dependent on the value of $\tilde{\omega}$. This can be circumvented by noting that since the term $(\sin\frac{\Omega N}{2})/(\sin\frac{\Omega}{2})$ does not change sign around $\Omega = 0$, the phase of $g(\omega_k - \tilde{\omega})$ in Eq. (8) is continuous with $\tilde{\omega}$. Therefore, an ingenious way of breaking down the $\hat{\omega} \leftrightarrow \hat{\theta}$ interdependency is to assume a first-order contribution from the phase of the $e^{-j\theta}g(\omega_k + \tilde{\omega})$ term in Eq. (8), and estimate the overall phase component $\tilde{\theta}$ by a linear interpolation of the DFT phase $Z(e^{j\omega_k})$ around the corresponding peak at $\omega_{\bar{k}}$, where there is an abrupt phase change. In this case, two situations may arise, as illustrated in Fig. 4, depending on the abrupt phase-drop starting (Case (a)) or ending (Case (b)) at $\omega_{\bar{k}}$, such that

$$\hat{\theta} = \frac{(\theta_b - \theta_a)\hat{\omega} + (\theta_a\omega_b - \theta_b\omega_a)}{\omega_b - \omega_a}, \tag{10}$$

with

$$\begin{cases} \text{Case (a):} & a \equiv \bar{k} \text{ and } b \equiv \bar{k} + 1 \\ \text{Case (b):} & a \equiv \bar{k} - 1 \text{ and } b \equiv \bar{k} \end{cases} \tag{11}$$

Once $\hat{\omega}$ and $\hat{\theta}$ are determined by maximizing Eq. (7), the amplitude estimate $\hat{a}$ can be determined by projecting the measured data onto the sinusoidal signal $\cos(\hat{\omega}n + \hat{\theta})$.

It is important to note that, if the sinusoid was complex, the interpolation of Eq. (10) would be exact. This is so because the theoretical spectrum would be given only by the term centered around $\tilde{\omega}$ on the right-hand side of Eq. (8). According to Eq. (9), this term has linear phase and is continuous as noted above.

Unfortunately, in the case of real sinusoids, the term centered around $-\tilde{\omega}$ interferes with the phase, and Eq. (10) becomes no longer exact. One can have an estimate of the kind of error committed when using this approximation by noting that the sum of two complex numbers in polar coordinates is given by:

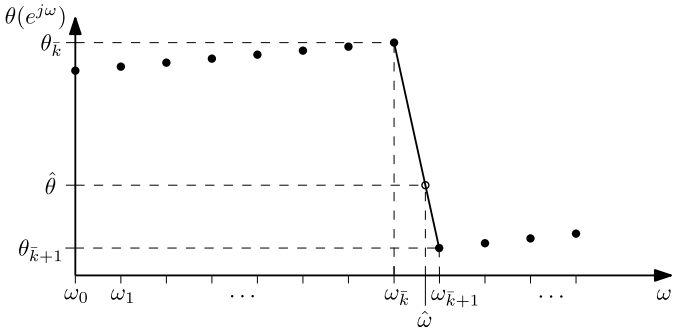

(a)

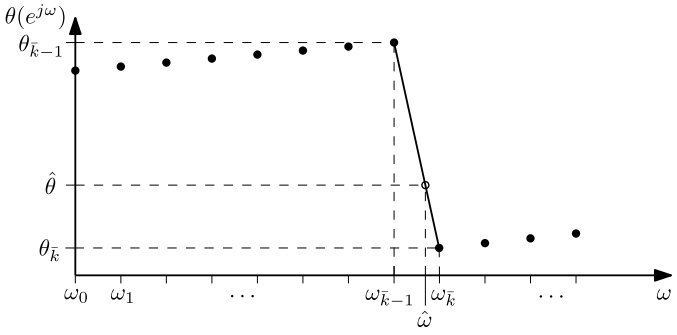

(b)

Fig. 4. Linear interpolation of DFT phase allows phase estimation with reduced computational cost for the estimated frequency value $\hat{\omega}$: (a) if the abrupt phase-drop starts at $\omega\bar{k}$; (b) if the abrupt phase-drop ends at $\omega\bar{k}$.

$$\rho e^{j\theta} = \rho_1 e^{j\theta_1} + \rho_2 e^{j\theta_2}, \tag{12}$$

where

$$\rho = \sqrt{\rho_1^2 + \rho_2^2 + 2\rho_1\rho_2\cos(\theta_1 - \theta_2)}, \tag{13}$$

$$\tan\theta = \frac{\sin\theta_1 + \frac{\rho_2}{\rho_1}\sin\theta_2}{\cos\theta_1 + \frac{\rho_2}{\rho_1}\cos\theta_2}. \tag{14}$$

Therefore, substituting $\tan\theta$ by the value given by Eq. (14), one has that

$$\tan(\theta - \theta_1) = \frac{\tan\theta - \tan\theta_1}{1 + \tan\theta\tan\theta_1} = \frac{\frac{\rho_2}{\rho_1}\sin(\theta_2 - \theta_1)}{1 + \frac{\rho_2}{\rho_1}\cos(\theta_2 - \theta_1)} \leq \frac{\frac{\rho_2}{\rho_1}}{1 - \frac{\rho_2}{\rho_1}}, \tag{15}$$

since $\sin x \leq 1$ and $\cos x \geq -1$.

Comparing Eq. (12) with Eqs. (8) and (9), one can see that ρ_1 is $|g(\omega_k - \tilde{\omega})|$, θ_1 is its associated (linear) phase, ρ_2 is $|g(\omega_k + \tilde{\omega})|$ and θ_2 is its associated phase, and θ is the overall phase. The error in the linear phase approximation is then given by $(\theta - \theta_1)$, that decreases with $\frac{\rho_2}{\rho_1} = |g(\omega_k + \tilde{\omega})|/|g(\omega_k - \tilde{\omega})|$. Provided that $|g(\omega_k - \tilde{\omega})| \gg |g(\omega_k + \tilde{\omega})|$, then $\frac{\rho_2}{\rho_1}$ is small and the linear approximation for the phase in Eq. (10) is quite reasonable. If $g(\Omega)$ is as in Eq. (9), the local maxima of its magnitude decrease with Ω. Since around $\tilde{\omega}$, $|g(\omega_k - \tilde{\omega})| \approx N$, the fraction $\frac{\rho_2}{\rho_1}$ is largest when $|g(\omega_k + \tilde{\omega})|$ is smallest. For example, if $F_s = 1000$ samples/s,

$\tilde{\omega} = 2\pi 20$ rad/s and $N = 512$ samples, then the value of $\frac{\rho_2}{\rho_1}$ is, for $\omega_{k-1} \leq \tilde{\omega}, \omega \leq \omega_k$, such that

$$\frac{\rho_2}{\rho_1} \approx \frac{|\frac{\sin(N\frac{\omega+\tilde{\omega}}{2})}{\sin(\frac{\omega+\tilde{\omega}}{2})}|}{N} \leq \frac{1}{N|\sin(\frac{\omega+\tilde{\omega}}{2})|} \leq \frac{1}{N|\sin(\frac{\tilde{\omega}-\Delta+\tilde{\omega}}{2})|}$$
$$\approx 0.018 \text{ rad} \approx 1^\circ. \quad (16)$$

A summary of the proposed MS algorithm is provided below:

1. Determine the N-point DFT, $Z(e^{j\omega_k})$, of the sequence $\mathbf{z}$ and find the position $\bar{k}$ of its magnitude maximum;
2. Set the neighborhood size $k_0 \geq 1$ around the magnitude maximum and determine the adjacent frequency values $\omega_k = k\frac{2\pi F_s}{N} = k\Delta$, with $(\bar{k} - k_0) \leq k \leq (\bar{k} + k_0)$, where F_s is the sampling frequency of $z(n)$ in samples/s;
3. `While` the iteration counter is smaller than or equal to a given number $I_{\max}$ of iterations `or` the variation of $\hat{\omega}$ in two consecutive iterations is below a certain precision threshold, `do`:
   (a) Estimate the phase component $\hat{\theta}$ using the frequency estimate $\hat{\omega}$ in Eq. (10), with θ_a and θ_b as defined in Eq. (11) and provided by the DFT $Z(e^{j\omega_k})$;
   (b) Determine the theoretical spectrum $S_{\hat{\omega},\hat{\theta}}(e^{j\omega_k})$, sampled at the $(2k_0 + 1)$ frequency points ω_k specified in Step 2, using the given values of $\hat{\omega}$ and $\hat{\theta}$ in Eq. (8);
   (c) Compute the correlation $\tilde{R}_{k_0}(\omega, \theta)$, as given in Eq. (7);
   (d) Perform one step of a golden-section search to upgrade the value of $\hat{\omega}$ in order to maximize the correlation function evaluated in the previous step.

   `End`.

5. Practical considerations

5.1. Algorithm initialization

An interpolation algorithm, such as the one in Section 3, may be used to provide the initial estimate for the proposed MS algorithm, due to its extreme simplicity and high precision. This reduces the number of line-search iterations and the associated evaluations of the correlation function given in Eq. (7).

5.2. Computational complexity

Following the description provided in end of Section 4, the computational complexity associated with the proposed MS algorithm includes:

- Step 1: An N-point DFT computation [18], which requires $(2 - \frac{3N}{2} + \frac{N}{2}\log_2 N)$ complex multiplications and $N\log_2 N$ complex additions, followed by the computation of its magnitude, which involves additional $(N + 2)$ real multiplications, $(\frac{N}{2} + 1)$ real additions, and $(\frac{N}{2} + 1)$ squared roots. Locating the maximum of this magnitude spectrum requires also $\log_2 N$ number comparisons;
- Step 2: Computing the frequency values ω_k, for $(2k_0 + 1)$ different values of k, requires $(2k_0 + 1)$ real multiplications;
- Step 3: For each of the $I_{\max}$ golden-section iterations:
  (a) 4 real multiplications and 4 real additions are employed to determine the value of $\hat{\theta}$ with Eq. (10);
  (b) 8 real multiplications, 8 sine/cosine computations, 2 real divisions, and 1 complex addition are used when implementing Eqs. (8) and (9) to determine each of the $(2k_0 + 1)$ spectrum estimates $S_{\hat{\omega},\hat{\theta}}(e^{j\omega_k})$;
  (c) $2(2k_0 + 1)$ complex multiplications, $4k_0$ complex additions, 1 squared root, and 1 complex division are required for determining $\tilde{R}_{k_0}(\omega, \theta)$ in Eq. (7).

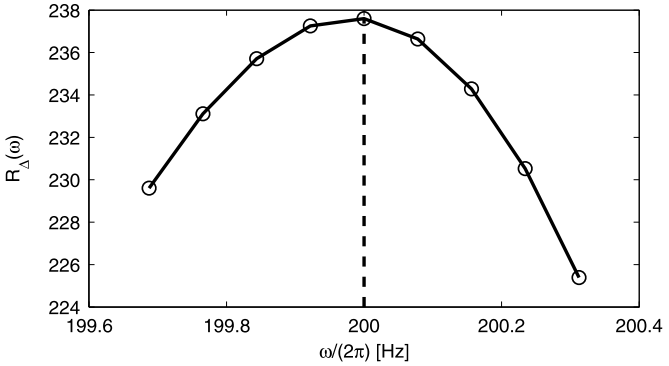

Fig. 5. Example of correlation function employed by the proposed algorithm. Its smooth profile, even for a low SNR = 5 dB, allows a simple line-search procedure to locate its maximum (indicated by dashed line) in a robust manner.

It is interesting to notice that Step 1 above is common to all other DFT-based algorithms such as the ML and interpolation-based ones. For the remaining stages, disregarding the complex/real nature of the operations, the MS algorithm requires, for instance, $(2k_0 + 1)(14I_{\max} + 1)$ multiplications. The most important aspect of this result is that the computational complexity of the optimization procedure of the MS algorithm is linear with k_0 and $I_{\max}$, whereas evaluating the ML objective function defined in Eq. (3) for $I_{\max}$ iterations is linear with N and $I_{\max}$, with $k_0 \ll N$ by several orders of magnitude. In addition, for large values of N, the additional MS operations required in Steps 2 and 3 above tend to be dominated by the initial DFT computation, which is also required by all algorithms considered here.

Therefore, in this entire process, two main factors affect the trade-off between the algorithm precision and computational complexity:

- The larger k_0, the larger is the complexity, and the more robust is the algorithm to noise, since the correlation in Eq. (7) is averaged over more points.
- The more iterations used in the line-search procedure to find the value $\hat{\omega}$ that maximizes the correlation, the more accurate are the estimations of $\tilde{\omega}$ and $\tilde{\theta}$. For example, in the present case, where the golden-section search is used, each extra iteration increases the frequency accuracy by $\phi \approx 1.62$.

5.3. Multiple sinusoids

The case of multiple sinusoids in the presence of noise can be dealt with an iterative approach as suggested in [19]. In that scheme, once a spectrum peak is identified, it is readily removed from the complete spectrum, allowing a more precise characterization of the remaining peaks. Once a new peak is identified and removed, however, all previous peaks are recalculated taking that new component into consideration. This process continues until all peaks have been properly identified.

To provide the reader with an idea of the behavior of the MS algorithm for two sinusoids, we have included in Section 6 an experiment with the estimation of the frequency of one sinusoid in the presence of an interference sinusoid whose frequency varies within a large range.

6. Experimental results

Experiment 1. We consider $N = 512$ samples of the signal $s(n) = \cos(\tilde{\omega}nT_s + \tilde{\theta})$, with $\tilde{\theta} = 25^\circ$, sampling frequency $F_s = 1/T_s = 1000$ samples/s, and distinct SNR levels.

For illustrative purposes, Fig. 5 depicts a typical profile of the correlation function defined in Eq. (7) during an execution of the

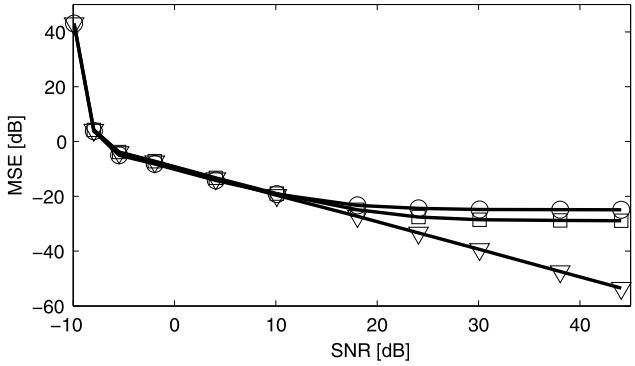

Fig. 6. Frequency MSE over 100 realizations within the frequency range $20 \leq \tilde{f} \leq 60$ Hz, in steps of 0.1 Hz, as a function of the SNR: ML ('○'), Interpolation [13] ('□'), and proposed MS ($k_0 = 1$, '∇') schemes.

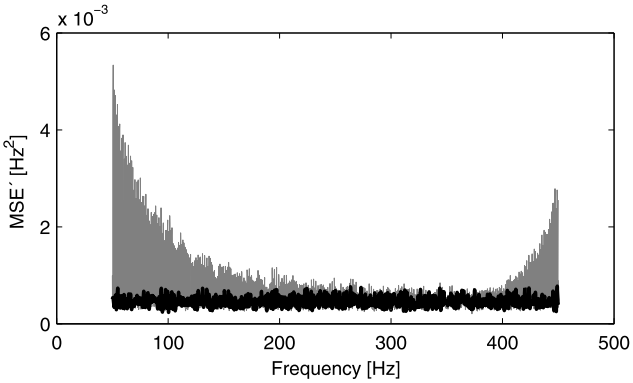

Fig. 7. Estimated frequency MSE′, over 100 realizations, as a function of the theoretical frequency for SNR = 24 dB: ML (gray) and proposed MS (black) algorithms.

Table 1
Frequency MSE [dB], for the entire frequency range $20 \leq \tilde{f} \leq 60$ Hz, as a function of the SNR for the ML, interpolation [13] (IM), and proposed MS (for $k_0 = 1, 3, 5$) methods.

SNR [dB]	ML	IM	MS		
			$k_0 = 1$	$k_0 = 3$	$k_0 = 5$
−9.9	43.0	45.0	43.0	43.0	43.0
−8.0	3.8	4.2	4.2	3.9	3.9
−5.5	−5.0	−3.8	−4.0	−4.8	−4.9
−1.9	−8.2	−7.2	−7.3	−8.0	−8.2
4.1	−14.2	−13.2	−13.5	−14.3	−14.5
10.1	−19.2	−19.0	−19.6	−20.3	−20.5
18.1	−23.3	−24.9	−27.3	−28.2	−28.4
24.1	−24.4	−27.5	−33.3	−34.2	−34.3
30.1	−24.8	−28.5	−39.3	−40.1	−40.3
38.1	−24.8	−28.8	−47.5	−48.2	−48.4
44.1	−24.9	−28.9	−53.5	−54.2	−54.3

proposed algorithm. The smooth profile of such a function enables a simple and robust algorithm to search for its desired peak in the proposed estimation algorithm.

The mean squared-error (MSE) of the estimated frequency $\hat{\omega} = 2\pi\hat{f}$ with respect to the correct frequency $\tilde{\omega} = 2\pi\tilde{f}$ is depicted in Fig. 6 for the ML, interpolation [13], and proposed MS (with $k_0 = 1$) algorithms. In this case, the MSE is determined over $N_r = 100$ realizations averaged across the frequency range $20 \leq \tilde{f} \leq 60$ Hz, in steps of 0.1 Hz, (totaling $N_q = 401$ distinct frequency values $\tilde{f}(q)$), such that

$$\mathrm{MSE}\,[\mathrm{dB}] = 10\log_{10}\left[\frac{1}{N_q}\frac{1}{N_r}\sum_{q=1}^{N_q}\sum_{r=1}^{N_r}\left(\hat{f}(q) - \tilde{f}(q)\right)^2\right], \tag{17}$$

with $\tilde{f}(q) = [20 + (q-1)0.1]$ Hz.

In this plot, one readily identifies the following MSE patterns within three distinct SNR regions:

- Low SNR (≤ -5 dB): In this range, the excessive noise causes a break-down behavior on all three algorithms, where the estimated frequency is quite distinct from the real one.
- Average SNR ($-5 < \mathrm{SNR} < 12$ dB): Here all resulting MSE decay linearly with the SNR level with a small ($\approx$1 dB) advantage for the ML algorithm, as detailed in Table 1. Such advantage, however, virtually disappears when we increase the value of k_0 in Eq. (7), even by a small amount, as also described in Table 1.
- High SNR ($\geq$12 dB): In this SNR range, the ML and interpolation algorithms present a saturation-like behavior, as the bias introduced by the aliasing components tend to dominate over the noise effect; meanwhile, the MS algorithm, by taking the alias into consideration in its model-based formulation, sustains the linearly decaying MSE behavior, as desired.

As observed in this experiment, the proposed MS algorithm tends to provide a more precise frequency estimate for high SNR values, what makes the algorithm perfectly suited for applications such as power-line quality monitoring [1], metrology [2–4] and so on. For lower SNR values, however, the MS algorithm may still be considered due to its reduced computational complexity, particularly when compared to the standard ML algorithm.

In Fig. 6, the algorithm performances are evaluated as a function of the SNR level, and the effect of the true-frequency $\tilde{\omega} = 2\pi\tilde{f}$ value is averaged over the entire interval $20 \leq \tilde{f} \leq 60$ Hz, generating a single MSE measure for each SNR value as defined in Eq. (17). The effect of the true $\tilde{\omega} = 2\pi\tilde{f}$ value on the MS and ML performances, as assessed by the figure of merit

$$\mathrm{MSE}'\left[\mathrm{Hz}^2\right] = \frac{1}{N_r}\sum_{r=1}^{N_r}(\hat{f} - \tilde{f})^2, \tag{18}$$

where $50 \leq \tilde{f} \leq 450$ Hz, averaged once again over $N_r = 100$ realizations, is depicted in Fig. 7 for a given 24-dB SNR level. From this plot, one observes how the ML frequency-estimate error increases when $\tilde{f} \approx 0$ and $\tilde{f} \approx F_s/2$, due to the aliasing effect of a nearby component $e^{-j\theta}g(\omega_k + \omega)$ in the real-sinusoid spectrum, as given in Eq. (8). This impulsive component does not affect the proposed algorithm's estimate as its effects are already taken into consideration on the original spectral model provided in Eq. (8), as explained above. This aliasing-free performance is the reason for the lower MSE provided by the MS algorithm, as seen in Fig. 6, particularly for higher SNR values. In the case of low SNR values, the estimate bias due to noise tends to dominate over this effect, leveling down the performances of the two algorithms.

The influence of N in the algorithm performances, as evaluated by the MSE defined in Eq. (17), is shown in Fig. 8 for $N_q = 1$ ($\tilde{f} = 50$ Hz, $\tilde{\theta} = 45°$, $F_s = 1000$ samples/s, and an SNR of 24 dB) and $N_r = 100$ realizations. In these low-frequency and high-SNR conditions, the MS algorithm consistently outperforms the interpolation-based and ML algorithms, as seen above, and a larger value number of samples N increases the DFT spectral resolution and, consequently, the algorithms' precisions accordingly.

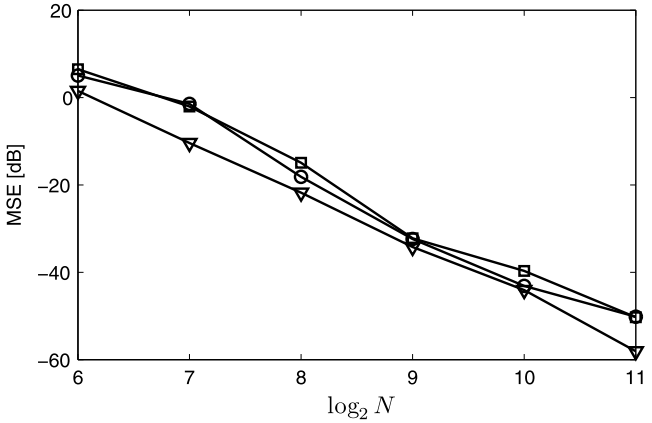

Fig. 8. Influence of number of samples N on the frequency MSE, over 100 realizations, for $\tilde{f} = 50$ Hz, $\tilde{\theta} = 45°$, $F_s = 1000$ samples/s, and an SNR of 24 dB: ML ('○'), Interpolation [13] ('□'), and proposed MS ($k_0 = 1$, '∇') schemes.

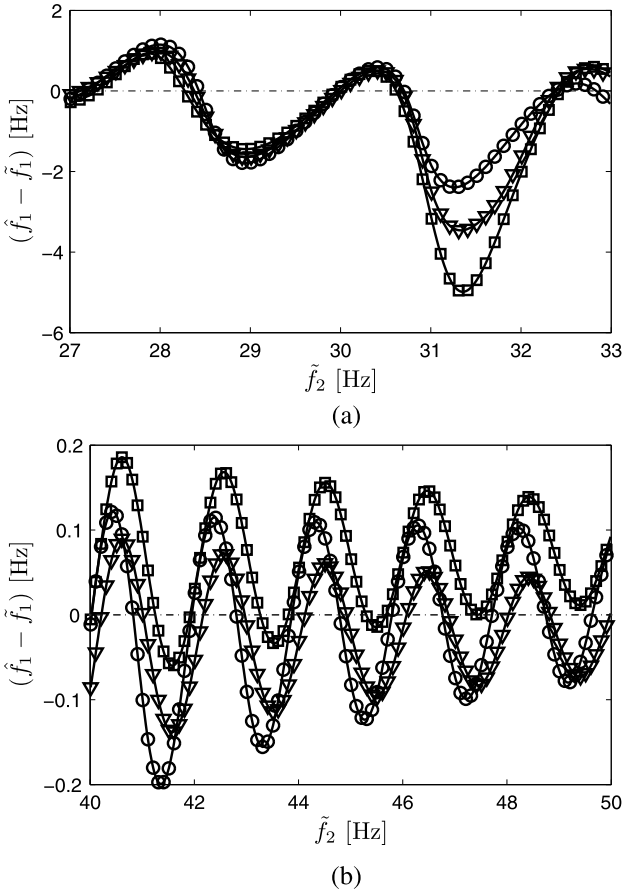

Fig. 9. Estimated frequency error $(\hat{f}_1 - \tilde{f}_1)$ in the presence of a second interfering sinusoidal component of frequency $\tilde{f}_2$ for ML ('○'), Interpolation [13] ('□'), and proposed MS ($k_0 = 1$, '∇') schemes: (a) $\tilde{f}_2 \approx \tilde{f}_1$; (b) $\tilde{f}_2 \gg \tilde{f}_1$.

Experiment 2. In this scenario, we investigate the algorithm performances in the presence of multiple sinusoids. For that purpose, we consider $N = 512$ samples of the signal $s(n) = \tilde{a}_1 \cos(\tilde{\omega}_1 n T_s + \tilde{\theta}_1) + \tilde{a}_2 \cos(\tilde{\omega}_2 n T_s + \tilde{\theta}_2)$, with $\tilde{a}_1 = 1$, $\tilde{\omega}_1 = 2\pi 30$ rad/s, $\tilde{\theta}_1 = 25°$, $\tilde{a}_2 = 0.5$, $\tilde{\theta}_2 = 75°$, sampled at a rate of $F_s = 1/T_s = 1000$ samples/s. The frequency estimate error $(\hat{f}_1 - \tilde{f}_1) = (\hat{\omega}_1 - \tilde{\omega}_1)/2\pi$ of the ML, interpolation-based and MS (with $k_0 = 1$) algorithms, for different frequency values $\tilde{\omega}_2 = 2\pi \tilde{f}_2$ of the interfering component, is shown in Figs. 9a (for $\tilde{f}_2 \approx \tilde{f}_1$) and 9b (for $\tilde{f}_2 \gg \tilde{f}_1$). From these plots, one observes the superior ML performance for $\tilde{f}_2 \approx \tilde{f}_1$, when the phase interaction from the two sinusoids affects the MS algorithm in a more significant way, whereas the MS algorithm prevails on the $\tilde{f}_2 \gg \tilde{f}_1$ case, when the spectrum-alias effect dominates the phase interaction, thus affecting the ML and interpolation-based performances. Increasing the value of k_0 (Eq. (7)), however, even by a small amount such as $k_0 = 3$ or $k_0 = 5$, improves the MS performance in all cases, making it similar to the MS performance when $\tilde{f}_2 \approx \tilde{f}_1$ and even better than already was when $\tilde{f}_2 \gg \tilde{f}_1$.

7. Conclusion

A matched-spectrum approach was introduced for the frequency-estimation problem. The proposed approach can efficiently take into account the spectral superposition that happens in real sinusoids, resulting in a very precise estimation at a computational cost comparable to the spectrum-interpolation methods. Numerical examples illustrate how the proposed scheme yields better frequency estimates, in comparison to both the standard maximum-likelihood and interpolation methods, particularly for high SNR levels and when the frequency of interest is near 0 or half the sampling-frequency value. These characteristics indicate the algorithm suitability for high-SNR applications, although low/medium SNR levels do not hinder the algorithm's performance in terms of estimation accuracy. In addition, it is important to notice that the precision and robustness of the proposed algorithm are scalable, and can be traded-off for computational complexity, as discussed above.

References

[1] M. Sedláček, J. Blaška, Low uncertainty power-line frequency estimation for distorted and noisy harmonic signals, Measurement 35 (2004) 97–107.
[2] E. Aboutanios, Estimating the parameters of sinusoids and decaying sinusoids in noise, IEEE Instrum. Meas. Mag. (Apr. 2011) 8–14.
[3] K. Duda, T.P. Zieliński, Efficacy of the frequency and damping estimation of a real-value sinusoid, IEEE Instrum. Meas. Mag. (Apr. 2013) 48–58.
[4] K. Duda, S. Barczentewicz, Interpolated DFT for $\sin^{\alpha}(x)$ windows, IEEE Trans. Instrum. Meas. 63 (4) (Apr. 2014) 754–760.
[5] J.-R. Liao, S. Lo, Analytical solutions for frequency estimators by interpolation of DFT coefficients, Signal Process. 100 (July 2014) 93–100.
[6] D.C. Rife, R.R. Boorstyn, Single-tone parameter estimation from discrete-time observations, IEEE Trans. Inf. Theory IT-20 (5) (Sept. 1974) 591–598.
[7] D.C. Rife, G.A. Vincent, Use of the discrete Fourier transform in the measurement of frequencies and levels of tones, Bell Syst. Tech. J. 49 (Feb. 1970) 197–228.
[8] J.O. Smith III, X. Serra, PARSHL: an analysis/synthesis program for non-harmonic sounds based on a sinusoidal representation, in: Proc. Int. Computer Music Conference, Tokyo, Japan, 1987, available at https://ccrma.stanford.edu/~jos/parshl/.
[9] J.C. Brown, M.S. Puckette, A high resolution fundamental frequency determination based on phase changes of the Fourier transform, J. Acoust. Soc. Am. 94 (2) (Aug. 1993) 662–667.
[10] M. Abe, J.O. Smith III, Design criteria for simple sinusoidal parameter estimation based on quadratic interpolation of FFT magnitude peaks, in: Proc. Audio Engineering Soc. Convention, San Francisco, USA, Oct. 2004, Audio Engineering Society, 2004, Paper # 6256.
[11] B.G. Quinn, Estimating frequency by interpolation using Fourier coefficients, IEEE Trans. Signal Process. 42 (5) (May 1994) 1264–1268.
[12] B.G. Quinn, Estimation of frequency, amplitude, and phase from the DFT of a time series, IEEE Trans. Signal Process. 45 (3) (Mar. 1997) 814–817.
[13] M.D. Macleod, Fast nearly ML estimation of the parameters of real or complex single tones or resolved multiple tones, IEEE Trans. Signal Process. 46 (1) (Jan. 1998) 141–148.
[14] E. Aboutanios, B. Mulgrew, Iterative frequency estimation by interpolation on Fourier coefficients, IEEE Trans. Signal Process. 53 (4) (Apr. 2005) 1237–1242.
[15] Y. Cao, G. Wei, F.-J. Chen, A closed-form expanded autocorrelation method for frequency estimation of a sinusoid, Signal Process. 92 (2012) 885–892.
[16] L.C. Palmer, Coarse frequency estimation using the discrete Fourier transform, IEEE Trans. Inf. Theory IT-20 (1) (Jan. 1974) 104–109.
[17] B.G. Quinn, I.V.L. Clarkson, R.G. McKilliam, Maximizing the periodogram, in: Proc. Globecom, 2008.

[18] P.S.R. Diniz, E.A.B. da Silva, S.L. Netto, Digital Signal Processing: System Analysis and Design, 2nd ed., Cambridge University Press, Cambridge, UK, 2010.
[19] P.T. Gough, A fast spectral estimation algorithm based on the FFT, IEEE Trans. Signal Process. 42 (6) (June 1994) 1317–1322.

Alessandro J.S. Dutra received the Electronics Engineer degree from Instituto Militar de Engenharia (IME) in 1991; the M.Sc. degree in Electrical Engineering from COPPE/UFRJ (1992), and the Ph.D. degree in Electrical Engineering from Rensselaer Polytechnic Institute (2010). Since 2012, he has been a researcher at General Electrics Research Center of Brazil.

José F.L. de Oliveira received the Electronics Engineer degree from the Federal University of Rio de Janeiro (UFRJ) in 1994; the M.Sc. degree in Electrical Engineering from COPPE/UFRJ in 1997, and the D.Sc. degree in Electrical Engineering COPPE/UFRJ in 2003. Since 2009, he has been a researcher at the Program of Electrical Engineering at COPPE/UFRJ.

Eduardo A.B. da Silva received the Electronics Engineering degree from Instituto Militar de Engenharia (IME), Brazil, in 1984, the M.Sc. degree in Electrical Engineering from Universidade Federal do Rio de Janeiro (UFRJ) in 1990, and the Ph.D. degree in Electronics from the University of Essex, England, in 1995. Since 1989 he has been with the Department of Electronics Engineering from UFRJ, and with the graduate Department of Electrical Engineering from COPPE/UFRJ since 1996. He is the co-author (with Paulo S.R. Diniz and Sergio L. Netto) of Digital Signal Processing: System Analysis and Design by Cambridge University Press, Cambridge, UK, 2nd edition, 2010.

Thiago de M. Prego received the Electronics Engineer degree from the Federal University of Rio de Janeiro (UFRJ) in 2007; the M.Sc. degree in Electrical Engineering from COPPE/UFRJ in 2009, and the D.Sc. degree in Electrical Engineering from COPPE/UFRJ in 2012. Since 2012, he has been with the he has also been with the graduate Program of Electrical Engineering at Federal Center for Technological Education Celso Suckow da Fonseca (CEFET-RJ) and he has also been a researcher at Program of Electrical Engineering at COPPE/UFRJ.

Sergio L. Netto received the Electronics Engineer degree from the Federal University of Rio de Janeiro (UFRJ) in 1991; the M.Sc. degree in Electrical Engineering from COPPE/UFRJ in 1992, and the Ph.D. degree in Electrical Engineering from University of Victoria, BC, Canada, in 1996. Since 1997, he has been with the undergraduate Department of Electronics and Computer Engineering at the UFRJ, and since 1998 he has also been with the graduate Program of Electrical Engineering at COPPE/UFRJ. He is the co-author (with Paulo S.R. Diniz and Eduardo A.B. da Silva) of Digital Signal Processing: System Analysis and Design by Cambridge University Press, Cambridge, UK, 2nd edition, 2010.